Stochastic and deterministic motion of a laminar-turbulent interface in a shear flow

Yohann Duguet[1], Olivier Le Maître[1], and Philipp Schlatter[2]

[1]*LIMSI-CNRS, UPR 3251, Université Paris-Sud, 91403 Orsay, France*

[2]*Linné Flow Centre, KTH Mechanics, SE-10044 Stockholm, Sweden*

(Dated: July 13, 2011)

Abstract

We investigate numerically the dynamics of a laminar-turbulent interface in plane Couette flow in the case where it is parallel to the mean flow direction. It is shown that the motion of the interface is essentially stochastic and can be modelled as a continuous-time random walk. Statistical analysis suggests a Gaussian diffusion process. The average speed of the interface and the corresponding diffusion coefficient are determined as functions of the Reynolds number Re, as well as the threshold value above which turbulence contaminates the whole domain. For the lowest values of Re, the stochastic dynamics competes with another deterministic regime of growth of the localised perturbations. The latter is interpreted as a depinning process from the homoclinic snaking region of the system. An extension of this interpretation to more general orientations of the interfaces is suggested.

1. INTRODUCTION

Transition to turbulence in wall-bounded flows has been a subject of intensive research for over a century. Many shear-induced flows fall into the class of *subcritical* transitional flows, i.e. excursions away from the laminar state can happen despite the linear stability of the underlying base flow. This necessarily points out the sensitivity of these flows to various kinds of disturbances with a finite amplitude. Closely associated to subcriticality is the observation that the effective transition to turbulence does not occur simultaneously at all locations in space, depending on the nature of the initial disturbances to the base flow. At any instant in time, the transitional flow can be formally described as the competition of two coexisting phases, namely the (absorbing) laminar and the (active) turbulent phase, separated by an unsteady interface with a dynamics of its own [1]. Early work by Emmons [2] shows that localised disturbances in boundary layers naturally evolve into organised patches called turbulent *spots*, fully localised in the in-plane directions. The border of a single turbulent spot is reported to expand with rather well-defined speeds which increase monotonically with the associated Reynolds number. In a certain parameter range, there has been evidence for stable laminar-turbulence coexistence since its experimental observation by Coles [3] and Van Atta [4] in counter-rotating Taylor–Couette flow. The interfaces were then surprisingly found to be oblique with respect to the principal flow direction. Obliqueness of the interfaces appears as a robust feature of spatially intermittent open flows near the onset of transition. Localised turbulent structures are also common in cylindrical pipe flow, they are called "puffs" when their streamwise length stays statistically constant and referred to as "slugs" when their length increases with time [5]. In all previous examples, the dynamics of the interface separating the laminar from the turbulent phase is highly unsteady. Understanding how such an interface evolves in space and time over long times is the key for predicting whether turbulence can eventually spread, be it partially, whether it will eventually recede, leaving the stable base flow as the unique equilibrium phase of the system, or whether patterns will emerge.

The present investigation focuses on the case of plane Couette flow (PCF), the incompressible flow between two parallel counter-sliding plates of infinite extent. The Reynolds number is defined here classically as $Re = Uh\nu$, where U, h and ν are the absolute velocity

of each plate, the half-gap between the plates, and the kinematic viscosity of the fluid, respectively. PCF is a convenient prototype for the study of subcritical transition since the associated base flow has a simple analytical expression $u(y) = Uy/h$ (with y the wall-normal coordinate) and is furthermore linearly stable for all values of the Reynolds number [6]. Its mean advection speed is zero which also enables easier tracking of disturbances. PCF experiments conducted in the early 1990's have focused on the dynamics of turbulent spots. Typically, though turbulent spots have been observed for Re as low as 280, they keep a finite probability to relaminarise up to $Re = Re_g \approx 325$ (see references [7],[8], [9], [10] and [11]). For $Re \geq Re_g$, a turbulent state is observed to compete with the metastable laminar regime as for the final regime. In the range $Re \in [325, 420]$, this turbulent regime is characterised by an incomplete contamination by the turbulent phase. When progressively moving away from Re_g, spatio-temporal intermittency becomes a dominant feature of the system, causing growing turbulent spots to split, merge and deform obliquely. The turbulent structure grows in a very unpredictable fashion, as shown by the oblique or labyrinthine patterns observed in experiments and in recent simulations [12–14]. Above $Re = Re_t \approx 420$, the growth of turbulent spots with time is best described as self-similar [15], their in-plane shapes being describable either as rhombs or as ellipses. Inside the turbulent spot and near its boundaries, the flow is locally dominated by streamwise-elongated streaks associated to counter-rotating streamwise vortices. Outside the localised spot, the velocity field departs slightly yet unambiguously from the laminar Couette flow, highlighting the presence of a robust large-scale secondary flow [15–17]. This secondary flow diverges away from the turbulent region in the spanwise direction, re-entering in the streamwise direction. It has been noted in several experimental studies that the side tip of a turbulent spot proceeds into the laminar region perpendicular to the main stream (the spanwise direction), suggesting a specific mechanism for the propagation of turbulence, called "growth by destabilisation" [18]. Difficulties in the interpretation of this specific mechanism arise naturally because of the many kinematic ingredients simultaneously at play: the streamwise streaks (spanwise modulations of the streamwise velocity, indicators of the turbulence), the in-plane secondary flow, as well as the mysterious presence of spanwise-propagating waves noted by several authors. It is thus desirable to find a convenient set-up where all these ingredients can be studied separately, with the hope that the resulting dynamics can shed light on the full mechanism. Noting that the secondary flow exists because of the localisation of the spot

3

in both in-plane directions, we will consider here the case where the laminar-turbulent interface is parallel to the streamwise direction. This is achieved using direct numerical simulation (DNS), by imposing periodicity in the streamwise directions, with a wavelength smaller than the typical streamwise extent of a localised spot. By doing so, the secondary flow is suppressed, while sustained streak-dominated turbulence is still possible. This choice should be seen as a numerical trick exploiting the advantages of Fourier-based spectral methods rather than as a limitation, as it enables one to investigate the spanwise propagation of turbulence independently from all other three-dimensional mechanisms. Obvious drawbacks due to the restraining geometry are the impossibility for oblique large-scale patterns to emerge, as well as artificially infinite velocity correlations along the streamwise direction inside the turbulent zone. As we shall see, even within this simplified framework the situation remains far from trivial because the fronts do not propagate with a constant velocity, necessitating a fully statistical treatment.

The paper is organised as follows: Section 2 contains a description of the dynamics observed in our numerical simulations for several values of Re. Section 3 focuses on the statistical analysis of front motion, culminating in the quantitative determination of the mean front speeds. Section 4 examines further the dynamics of the fronts for the lowest values of Re analysed previously and highlights a radically different (deterministic) propagation mechanism. All the results, as well as their extension to generic shapes of laminar-turbulent interfaces, are eventually discussed in Section 5.

2. DIRECT NAVIER–STOKES SIMULATIONS

2.1 Numerical procedure

In this paper we use the classical notations to describe the geometry of plane Couette flow. The fluid is sheared between two parallel plates of velocities $\pm U$ in the streamwise direction x, separated by a gap $2h$ in the wall-normal direction y. The spanwise direction is denoted z. The three-dimensional flow is governed by the incompressible Navier–Stokes equations with no-slip boundary conditions at both walls. Velocities, space and time are

4

non-dimensionalised by U, h and h/U, respectively. The spectral representation of the flow is based on Chebyshev polynomials in the y-direction, and a discrete Fourier decomposition in both x and z [19]. This implies periodic boundary conditions in the in-plane directions, with the associated wavelengths denoted L_x and L_z, respectively. Time-stepping is achieved by a fourth-order Runge-Kutta integrator with adaptive variable timestep. The number of spectral modes is determined by the triplet $\boldsymbol{N} = (N_x, N_y, N_z)$, with the extra use of the 3/2-dealiasing rule for the evaluation of the nonlinear terms in the wall-parallel directions.

We perform well-resolved simulations in a domain $D1$ of size $(L_x, L_z) = (10.417, 250)$, using a resolution $\boldsymbol{N} = (32, 49, 1024)$. For the simulations at the lowest values of Re, the slow spreading of localised perturbations made it possible to use a shorter domain $D2$ of size $(L_x, L_z) = (10.417, 125)$ with half the number of collocations points in the spanwise direction, *i.e.* $\boldsymbol{N} = (32, 49, 512)$. The short streamwise extent L_x is used as a numerical trick forcing potential laminar-turbulent interfaces to be orthogonal to the spanwise direction z, preventing the formation of a secondary large-scale flow around localised spots. The value of ≈ 10 has been selected because it is of the order of magnitude of the wavelength of the streak instabilities observed near the spanwise tips of turbulent spots (see Ref. [15]). Larger wavelength instabilities responsible for potential shape modulations of the front are naturally excluded from the current analysis study as they are expected to be one order of magnitude larger and to be driven by the dynamics of the large-scale secondary flow.Note that a similar geometry has been used by Barkley & Tuckerman [20] (Fig. 15) in quenching experiments with $(L_x, L_z) = (10, 120)$ down to $Re \approx 210$. More recently, edge states and other spanwise localised finite-amplitude solutions were found in a similar geometry with $(L_x, L_z) = (4\pi, 8\pi)$ [21] and $(4\pi, 16\pi)$ [44].

Several types of initial perturbations of the base state were used in the course of the present investigation, either localised or not. Localised conditions are identical to the ones used by Duguet *et al.* [23], yet with a possible prescribed rotation around the y-axis in order to break the initial symmetry. At high enough Re and when applied with a sufficiently large amplitude, those localised perturbations lead to a turbulent flow localised in the z-direction, which for convenience will be referred to as a "spot" for this system (though strictly speaking, a real "spot" should be also localised in the x-direction). For a given value of Re, it is also possible to use a spot generated at another (generally higher) value of

Re as an initial condition. Exploiting the subcritical nature of the system, this second type of disturbance will be used mostly at the lowest value Re in order to increase the chances of effectively triggering turbulent motion.

Identification of the fronts

Simulations were performed for Re in the range $[180, 650]$ and with computational domains $D1$ or $D2$. Typical traces of $v_{rms}(t)$ on a time interval $[0, 1500]$ are shown in Fig. 1 for various values of Re. Here, as in Duguet *et al.* [12], v_{rms} stands for the root mean square of the $y-$component of the velocity. Note that $v_{rms} = 0$ denotes a globally laminar flow so that v_{rms} can safely be interpreted as a measure of the spatial spreading of the turbulence, weighted by its local intensity. From the fig. it is clear that for $Re > 500$, v_{rms} rapidly increases both with time and with Re, though the increase with time is not strictly linear. For Re betwen 400 and 500, the signals contain more high-frequency components when Re increases, while the average growth becomes slower for decreasing Reynolds. For Re below 400, the average increase in v_{rms} is hardly noticeable on the time span shown here, suggesting that turbulence spreading, if ever, occurs only in an intermittent way. Finally, for $Re < 280$, signals of $v_{rms}(t)$ become extremely smooth, almost time-periodic, with a finite possibility for sudden complete relaminarisation as seen here for $Re = 210$. For those values the signal is so smooth that the dynamics can difficultly be termed 'turbulent' in the light of Fig. 1. The fact that non-trivial dynamics can be sustained for long times for surprisingly low values of $Re \approx 200$ was already documented in earlier computations where Re was decreased by steps [20].

Because of the choice of a domain having a small extension L_x, the flow geometry is nearly one-dimensional. It is thus convenient to analyse the motion of the fronts using snapshots of the velocity field at a given streamwise location, say $x = 0$. Visualisation of the dynamics is helpful for determining a relevant criterion for the identification of the laminar-turbulent interface. Fig. 2 shows a selected part of the domain $D1$ during the spreading of a spot at $Re = 500$, the displayed quantity being the total streamwise velocity $u = u(x = 0, y, z)$ at time $t = 694$. The main part of the picture is characterised by nearly z-periodic undulations of the iso-lines of u which are typical of turbulent streaks.
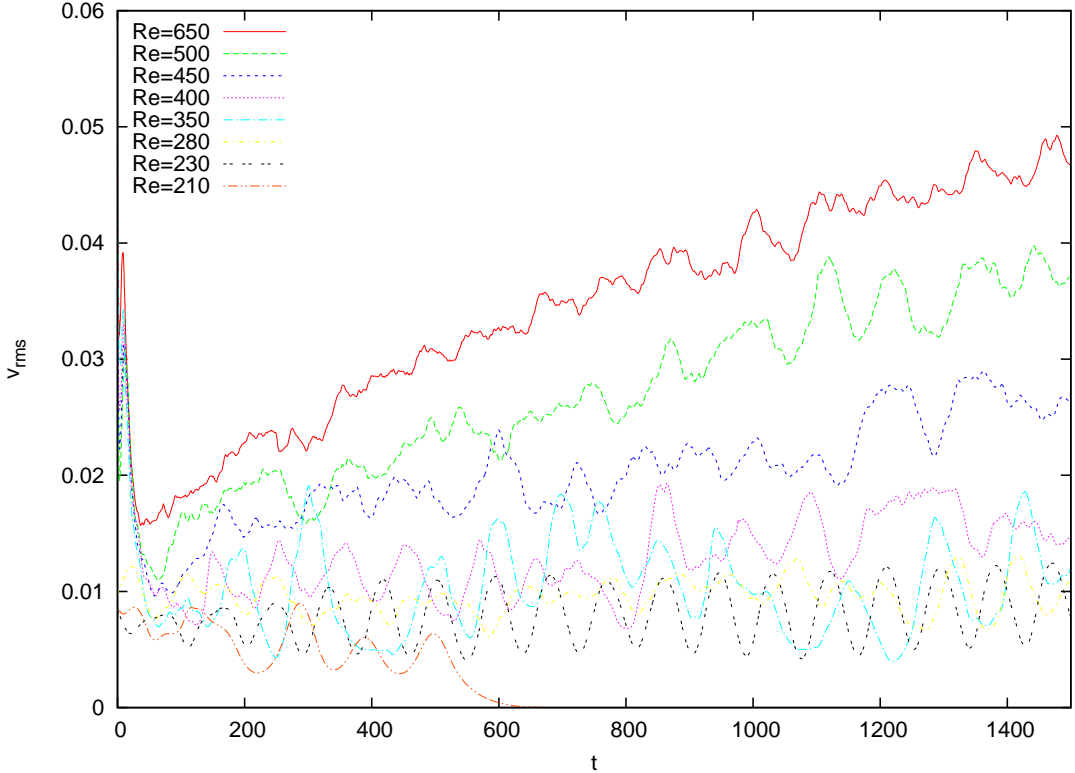
FIG. 1: Wall-normal root mean square velocity *vs* time for several values of Re

These undulations are marked by narrow zones, staggered on either wall, where the near-wall value of $u \approx \pm 1$ penetrates deeper into the flow towards the opposite wall, indicative of local bursting events. Such bursting events are reminiscent of the mechanism unfolded in Refs [24–26] in terms of dynamical systems, yet here in the context of a wide domain allowing for the presence of an interface. The spanwise wavelength of these undulations is approximatively equal to 4 but is far from being strictly constant [27]. This turbulent zone extends here from the left of the picture ($z = 0$) up to $z \approx 45$ where all iso-lines become parallel and equi-spaced, indicating the laminar base flow. The front delimiting the laminar from the turbulent phase in Fig. 2 is thus located at $z \approx 45$. Note that this single snapshot is *a priori* indistiguishable from the slice through a fully localised spot. Magnification of the region $z \in [35, 47]$ is shown in Fig. 3 in order to reveal the temporal dynamics associated with the motion of the front for $t \in [610, 710]$. The sequence reveals that each of the detached regions oscillates in a rather unpredictable way, but that its location remains steady. The steady location of the streaks now distinguishes this system from the systems with large L_x, where all streaks near the fronts are advected away (see Fig.7 in Ref. [9]). This
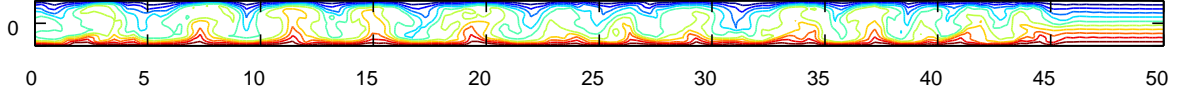
7

FIG. 2: Streamwise velocity, $Re = 500$, $t = 694$, case (A), real aspect ratio.

discrepancy between simulation in the domain $D1$ and experimental findings is nothing but the expected manifestation of the confinement in the x-direction, supressing the secondary flow which advects the streaks away in the spanwise direction. Now focusing on the dynamics near the interface, we can isolate the mechanisms responsible for the progression in z of the interface. For $t = 610$ (Fig. 3), only three ejections (upwards or downwards) of streamwise velocity can be observed, staggered on either wall. The rightmost ejection is located at $y = -1$, $z = 41$ and faces quasi-laminar flow on the opposite wall at $y = +1$. For $t = 629$ four ejections are present in the figure, one additional ejection being at $y = +1$, $z = 42$, now facing quasi-laminar flow on the opposite wall at $y = -1$. The pre-existing streaks stay at their initial location, thus the advancement of the front between $t = 610$ and 629 must correspond to the generation of a new streak at the opposite wall and not to a propagation of the streak pattern. The sequences of intermittent generation events displayed in Fig. 3 suggests a contamination process occuring as follows. When a fluid ejection from one wall is sufficiently intense, it affects the opposite wall, inducing there a compression of the iso-lines. Because of the incompressibility constraint, the low-velocity fluid near that wall is deviated towards both positive and negatives x-locations. This generates a deficit velocity in the previously laminar zone near the same wall, in other words a new streak. The process then starts again to contaminate the opposite wall as soon as a sufficiently large bursting event occurs. This scenario highlights two facts: firstly, the motion of the front occurs via discrete events, $i.e.$ progress of the interface is not continuous but occurs on a finite distance at given times. Secondly, weak fluid ejections are not sufficient to generate new streaks, as shown by the aborted bursting event in Fig. 3 between $t = 644$ and $t = 680$. This suggests that the motion of the front is due to local finite-amplitude instabilities of the flow, and not to any linear instability of the flow at some distance away, as would be the case for pulled fronts [28]. Note that this scenario relies on the presence of two walls, and its extension to boundary layer flows (involving only one wall) remains an open question.

In competition with the generation process displayed in Fig. 3, there are also retreat
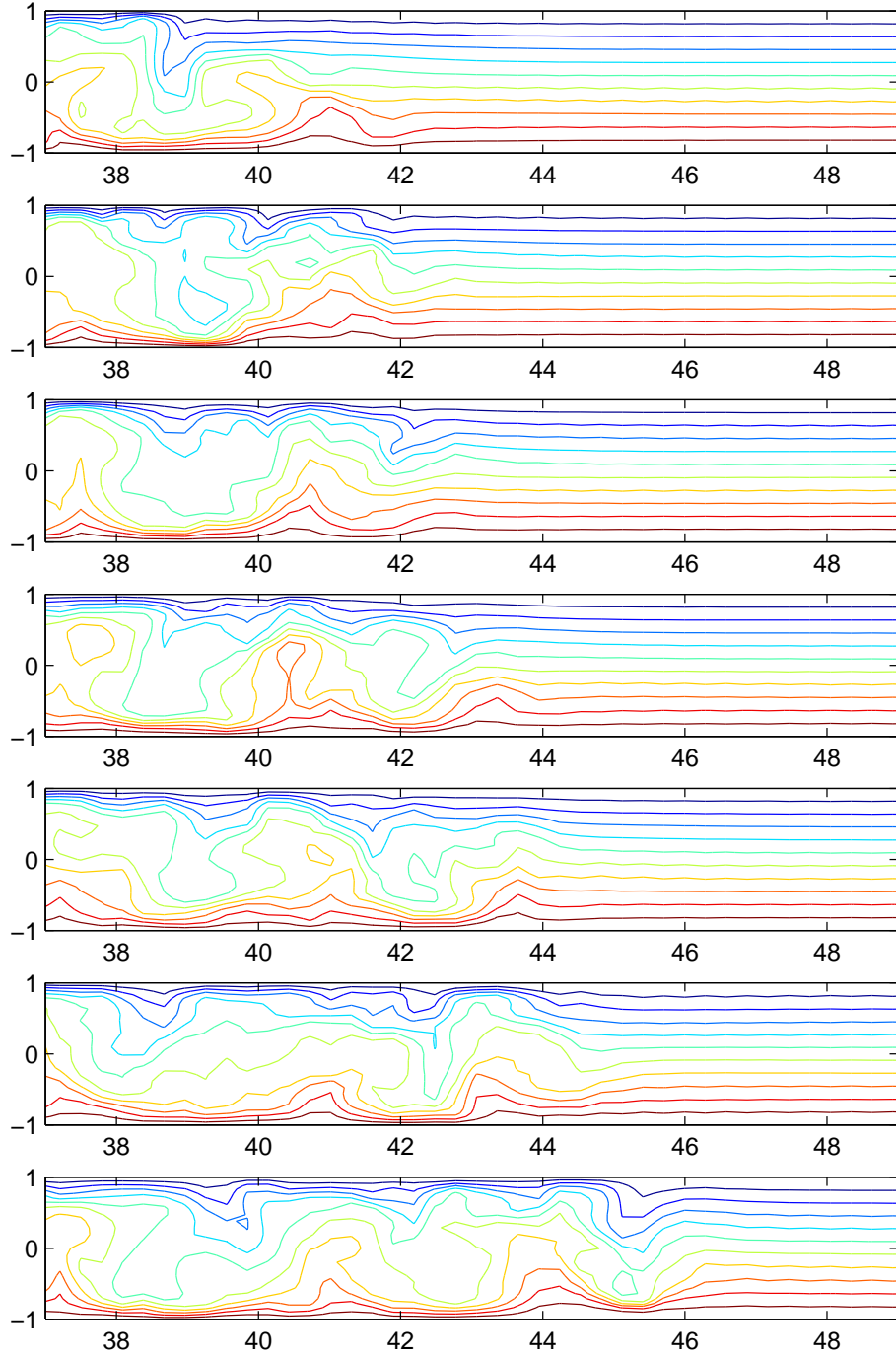
FIG. 3: Spanwise development of a turbulent spot at $Re = 500$. Total streamwise velocity field in the plane $x = 0$ at times $t = 610,\ 624,\ 629,\ 644,\ 660,\ 680$ and 710.

events where streaks near the interface disappear because the turbulent intensity has not proven sufficiently large to sustain the streak. Intuitively, at large values of Re the turbulent activity inside the boundary layers is intense, which will favour efficient bursting events and

9

a rapid propagation of the front, while at low values of Re aborted bursting events will dominate, forcing the front to retract.

The location of humps in the iso-lines appears as a natural means to identifying visually streaks and the associated turbulent dynamics. In particular, the $u = 0$ isoline, which is at $y = 0$ where the flow is laminar, is deviated towards one of the wall according to the upwards or downwards ejections occuring near a wall at the same z-location. The y-coordinate of this iso-line $u = 0$ then appears as a convenient measure of the local deviation from laminar flow. Yet in order to avoid x-dependent quantities, we exploit the assumption of small L_x and average over x the streamwise velocity u. We thus define the quantity $Y(z,t)$ as the wall-normal coordinate of the isovalue $\langle u \rangle_x = 0$, where $\langle u \rangle_x(y, z, t)$ is the x-average total streamwise velocity field, i.e.:

$$Y(z,t) = \{y | \langle u \rangle_x = 0\}. \tag{1}$$

Note that $Y(z,t)$ may not be uniquely defined if the distortion of the flow from the laminar one is important such that $\langle u \rangle_x(y, z, t)$ has multiple zeros in y. During the course of this investigation we have not stumbled on any difficulty related to an ill-posed definition of the quantity Y, owing to the range of Re considered for which ejections remain rather mild. Typical space-time diagrams of $Y(z,t)$ are shown in Figure 4 for two simulations using two types of initial conditions. The first simulation corresponds to the evolution of an initially localized turbulent burst at $Re = 370$ (left plot) and the second corresponds to the evolution of a homogeneous turbulent field at $Re = 280$ (right plot) where the initial condition is the results of a simulation at higher Re.

An open issue remains the choice of an appropriate threshold value Y_c to distinguish laminar from turbulent domains. Owing to the absence of large scale secondary flow, as discussed in the Introduction, a sharp (faster than exponential) decay with z of all perturbation velocity components away from the interface in the laminar domain is observed, hence the proposed definition of the interface is rather insensitive to the specific choice for Y_c. Taking $|Y_c| = 0.2$ in absolute value has proven a robust choice for the practical threshold criterion in the definition of turbulence domains. The robustness of the analysis with regard to the selection of the threshold value Y_c is further discussed in the following section.
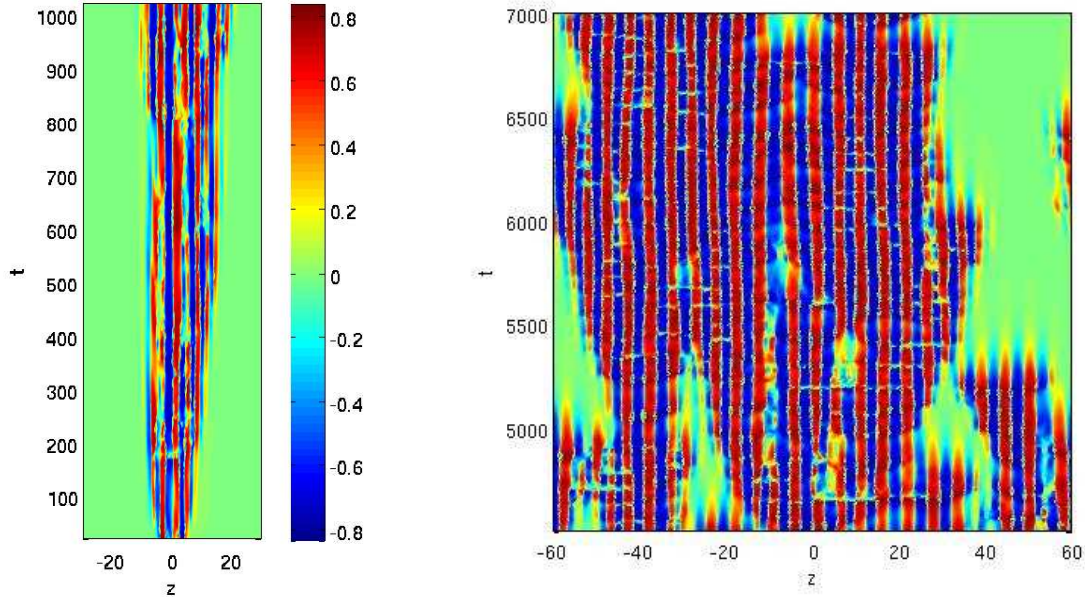
FIG. 4: Space-time (z, t) diagrams for the quantity $\{y \mid \langle u \rangle_x = 0\}$; $Re = 370$ from a localised initial condition (left) and $Re = 280$ from a homogeneous turbulent initial condition (right).

3. STOCHASTIC MODELLING OF FRONT MOTION

3.1 The motion of the interface as a continuous time random walk

A large number of simulations has been performed, starting from either a localised disturbance or from a turbulent field at higher Re as shown in Figure 4. The analysis is based on space-time (z, t)-diagrams of the quantity $Y(z, t)$ defined in Eq. (1). All the diagrams shown here are computed on a grid with spatial steps $\Delta z = 0.2$ and $\Delta t = 5$. The diagrams shown in Fig. 5 correspond to one simulation at $Re = 380$. The top plot shows the colour-coded values of $Y(z, t)$. It is clear that the uniformly green areas where $Y(z, t) \approx 0$ corresponds to laminar areas, whereas the central domain where $Y(z, t)$ significantly deviates from 0 corresponds to the turbulent spot. Using the criterion discussed above, we can extract the iso-lines $Y(z, t) = \pm 0.2$ to better appreciate the structure of the turbulent spot and its dynamics. The turbulent zone is here delimited by two asymmetric fronts. Each of the two fronts clearly moves from or towards the turbulent area in discrete steps, gaining or losing one streak (occasionnally several streaks at once). The time interval between two successive events is variable, requesting a statistical description. The distance along which the front

11

has advanced or retreated during one of these events is also not constant, firstly because streaks do not possess a uniquely defined spanwise size, secondly because several streaks can be gained or lost within a single "event". A convenient description of the motion of each front, well-adapted to a statistical description, is within the frame of continuous-time random walks (CTRW) [29]. Retreat and progress of a given interface are seen here as two competing and complementary events occuring suddenly after a time T ("the waiting time") on a distance Δz (the "jump length") . The CTRW process is here asymmetric, because the events "gaining" and "losing" streak(s) are not equiprobable, inducing statistically a drift of each front in one direction or the other. In the following, we shall use subscripts g to refer to growth events ("gaining streaks") and r to retreat events ("losing streaks"). We shall assume that the random dynamics of the interface is a memory-less stochastic process, homogeneous in time and space. It implies that waiting times and jump magnitudes for r and g events are statistically independent. With these assumptions, four cumulative probability distributions are needed to fully characterise the random dynamics of interface:

- $P_{T_g}(T > t)$ (resp. $P_{T_r}(T > t)$) : the probability that, the next event being a *growth* (resp. *retreat*) event, it occurs after a waiting time T is larger than a time $t > 0$,

- $P_{\Delta_g}(\Delta z > L)$ (resp. $P_{\Delta_r}(\Delta z > L)$): the probability that, the next event being a *growth* (resp. *retreat*), the magnitude of the jump Δz is larger than $L > 0$.

It is remarked that, because of the periodic conditions, fronts necessarily go by pairs, forming at least one localised spot. Also, the probabilities $P_{\Delta_{g,r}}$ concern the (unsigned) jump magnitudes and it will be necessary to introduce below their signed or oriented counterparts, adopting a convention on the sign of Δz depending on the type r or g of the event.

Note that the CTRW approach is only one possibility of modelling the motion of the interface with the available data, and that it corresponds to a deliberate choice for a modelling strategy. Whether such a description of the front motion is relevant for all values of Re has to and will be discussed. Another modelling options, not discussed here, is the directed percolation approach using probabilistic cellular automata, for which a large body of literature exists in the case of quasi-one dimensional systems such as ours (see e.g. Ref. [30]). One reason to discard that approach in this investigation is that it would also require accurate statistics of the laminar gaps forming within the system. This appears uselessly costly given

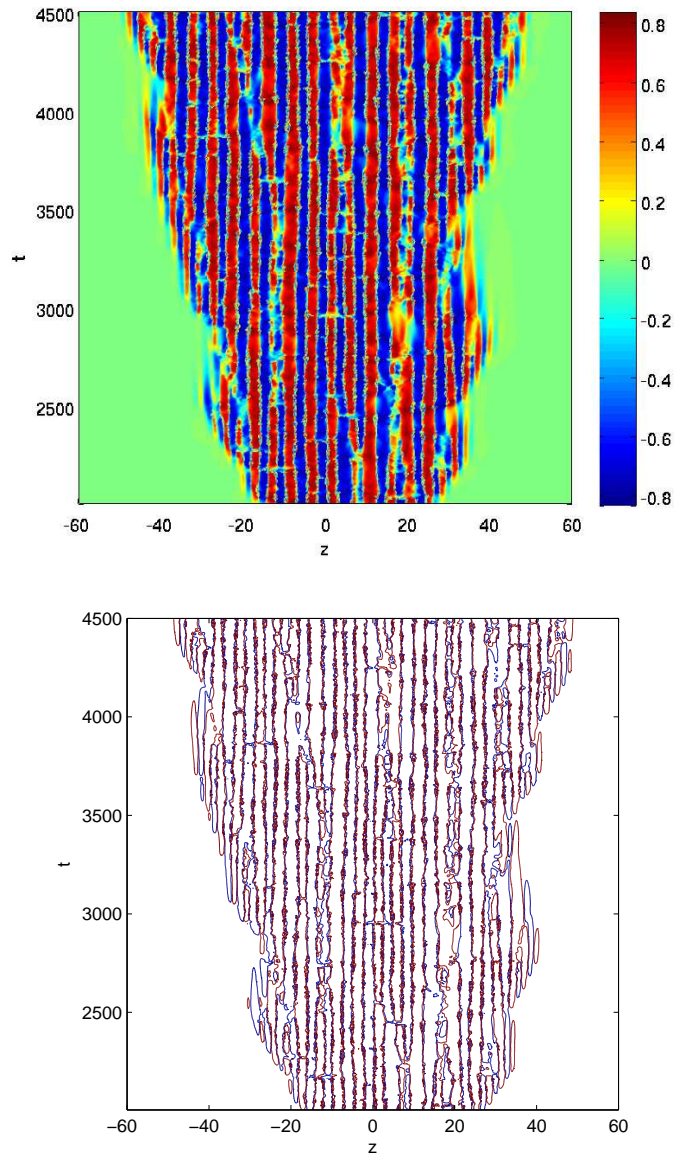the conclusions we wish to draw from this study, namely the average front velocity as a function of Re.

FIG. 5: Space-time diagrams for the quantity $Y(z,t)$ (see text)for $Re = 380$. Top: Iso-contours of $Y(z,t)$ ranging continuously from -1 to 1. Bottom: Iso-contours $Y(z,t) = \pm 0.2$

3.2 Analysis of the front dynamics

For each value of Re in the range $[230, 650]$, we performed independent simulations varying the initial conditions to obtain space-time diagrams such as in Figure 5(b). Each of these
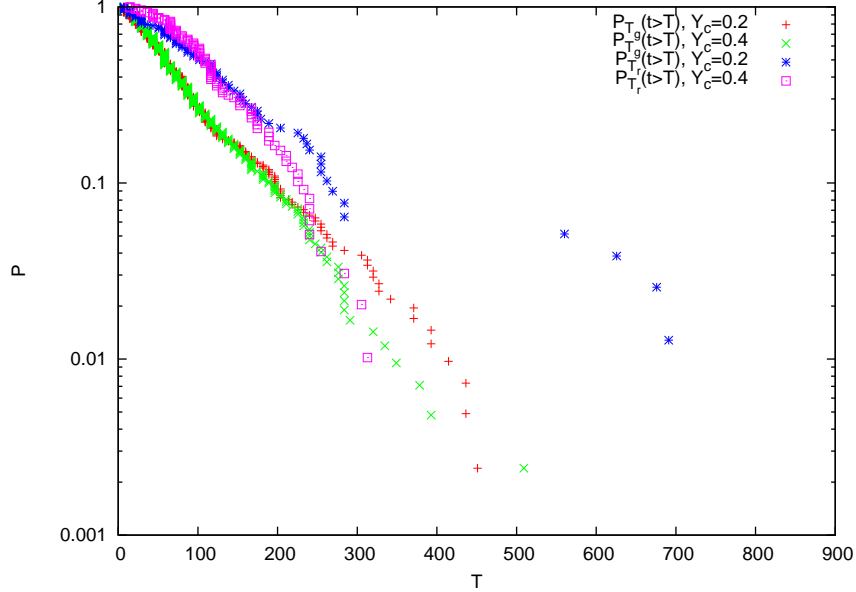
13

FIG. 6: Probability distributions for the waiting times $P_{T_g}(T > t)$ and $P_{T_r}(T > t)$ for $Re = 380$ and two values of the threshold Y_c.

diagrams was subsequently automatically treated to detect laminar-turbulent interfaces and extract waiting times and magnitude of the jumps, sorted by r or g events. All the data were then collected to construct the four empirical distribution functions. Let us begin by describing the distributions for the waiting times T. Figure 6 gathers data from several simulations at $Re = 380$; the data suggest clearly that the distributions P_{T_g} and P_{T_r} can be well fitted by exponential distributions. This suggests a Poisson distribution for the waiting times regardless of which event is considered (g or r), confirming the memoryless character of the dynamics. Note that the exponential behaviour is more convincing for P_{T_g} than for P_{T_r} as the tails of the distributions are better converged for the former; it simply reflects the fact that g-events are more probable for $Re = 380$ than r-events. Figure 6 also compares the distributions obtained using two values for the criterion $Y_c = 0.2$ and $Y_c = 0.4$; it is seen that the selected value for Y_c has a marginal impact on the resulting empirical distributions of the waiting times, in the sense that the discrepancies in the slopes are within the acceptance range (of the order of the interpolation errors).

The empirical distributions of the waiting times corresponding to the values of Re investigated are gathered in Figure 7. A clear Poissonian trend emerges for P_{T_g} (top-plot of Figure 7) at $Re \geq 300$, with the slope montonously increasing with increasing Re. The

14

cases $250 \leq Re \leq 290$ are less clearly amenable to an interpretation as a memory-less process, because of the presence of extreme events (very long waiting times). The data are here insufficient to decide whether the extreme events only produce unconverged statistics (still ruled by Poissonian dynamics) or if a second tail is emerging with a different scaling [31]. For $Re = 230$ and less (not shown), the global deviation from exponential distribution is large, suggesting a different process and motivating the analysis presented in Section 4. Description of the retreat waiting time distribution P_{T_r} (bottom plot of Figure 7) reveals the same trends, however the slopes increase with increasing Re. Furthermore, the analysis is blurred at high Re by the rarity of retreat events compared to growth events: above $Re \geq 400$, the occurence of retreat events would demand too much simulation time (or equivalently too many independent simulations) to produce converged statistics. In what follows, we will suppose that for $Re \geq 400$, the waiting time of r-event is exponentially distributed with mean $\langle T_r \rangle = +\infty$, i.e. retreat events never occur.

Similar observations hold for the empirical distributions for the magnitude of the r and g jumps reported in Figure 8. Specifically, exponential distributions can be reasonably assumed if one neglects rare events for the lowest Reynolds values. The implications of this finding are important: as long as the exponential scaling holds, the motion of the front can be thought of as a Gaussian (normal) diffusion process. In particular, there is little ambiguity that the distributions do *not* follow a power-law behaviour, thus excluding a description in terms of Levy flights and anomalous diffusion processes.

For a Poissonian distribution of the form $P(X > x) \sim e^{-\frac{x}{a}}$, logarithmic interpolation of the slope directly yields its average value $\langle X \rangle = a$. We exploit this property to graphically estimate the average waiting times $\langle T_g \rangle$ (resp. $\langle T_r \rangle$), i.e. the average waiting time given that the next event is a g event (resp. a r event). Figure 9 presents the computed average waiting times of the two r and g events as functions of Re, obtained by fitting the empirical distributions shown in Figure 7. The error bars are constructed to graphically bracket the empirical distributions and to account for some arbitrariness in disregarding rare events. Figure 9 shows that the average waiting time $\langle T_g \rangle$ monotonically decrease with Re while $\langle T_r \rangle$ monotonically increases with Re. The two averages thus cross at a given value of Re, $Re_{c1} = 320 \pm 10$. The interpretation is straightforward: for $Re > Re_{c1}$, the probability is higher that the next event will be a growth event rather than a retreat event, regardless
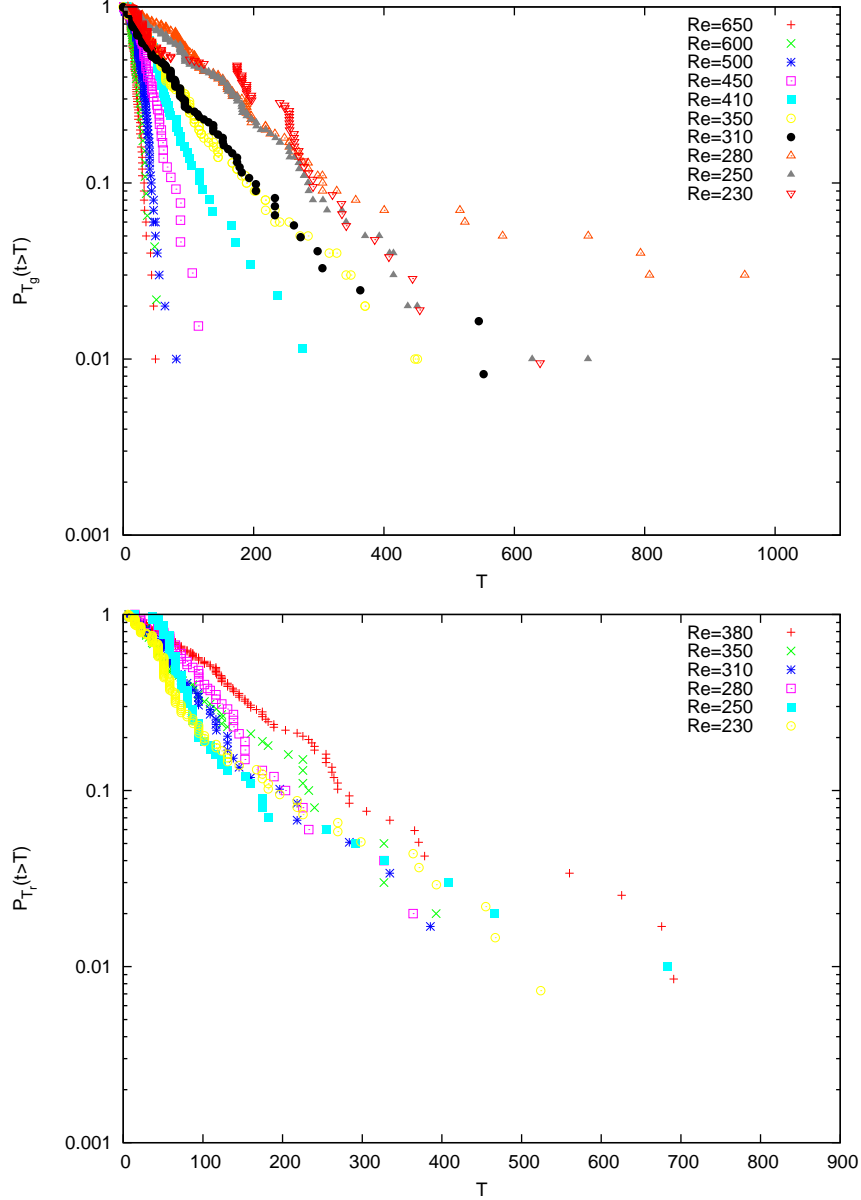
15

FIG. 7: Cumulative probability distributions for the waiting times $P_{T_g}(t > T)$ (top) and $P_{T_r}(t > T)$ (bottom) for various values of Re.

of the history of the front, while retreat events are favoured statistically for $Re < Re_{c1}$. The two average times coincide exactly only for $Re = Re_{c1}$. There is a strong analogy with the formalism adopted in studies of intermittent pipe flow, where single turbulent puffs can statistically undergo complementary events, as they either relaminarise or split [32, 33]. We observe that Re_{c1} is strikingly close to the experimental threshold $Re_g \approx 325$ in large domains [9, 12].
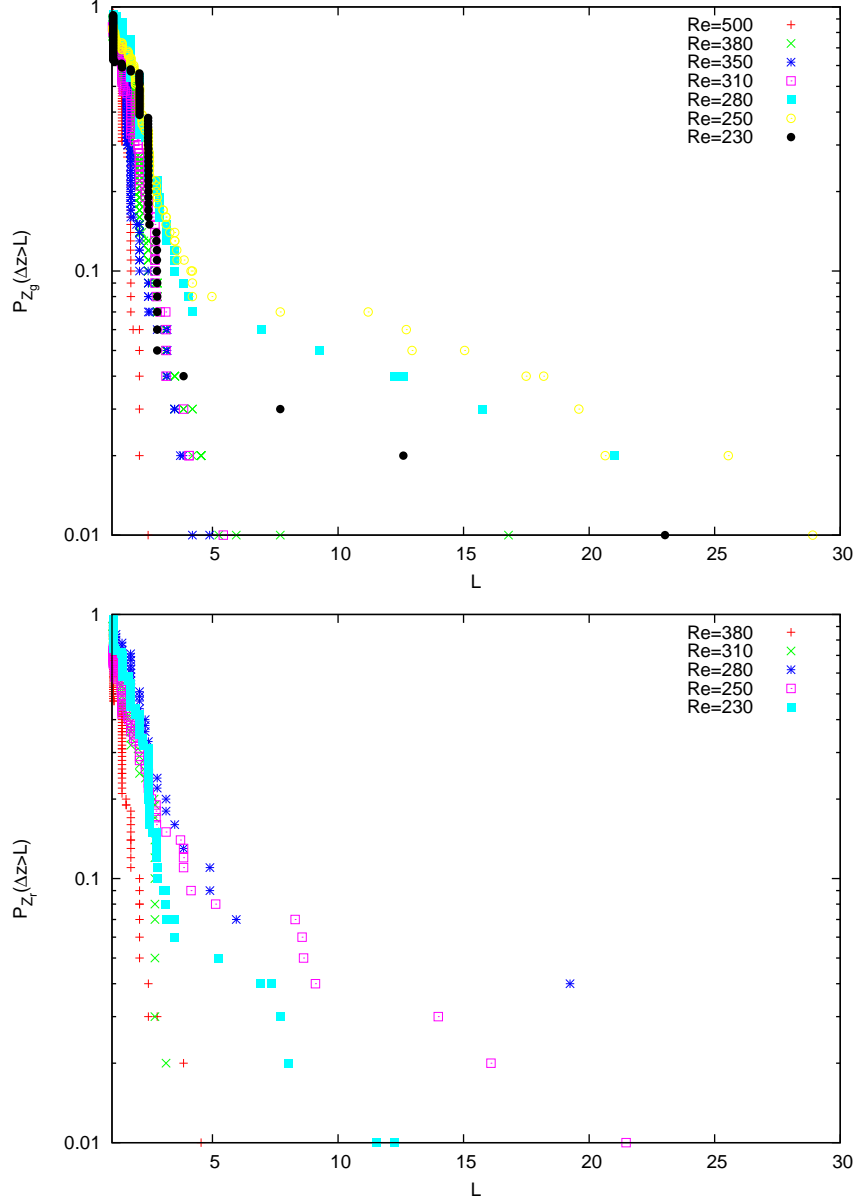
FIG. 8: Cumulative probability distributions for the jump lengths $P_{Z_g}(\Delta z > L)$ (top) and $P_{Z_r}(\Delta z > L)$ (bottom) for various values of Re.

Strictly speaking, this does not mean that the front is statistically steady at $Re = Re_{c1}$, nor that the turbulent domain statistically expands for $Re > Re_{c1}$ or retracts for $Re < Re_{c1}$, since the jump length distributions must also be included in the picture. Equivalently to the waiting times, the conditional averages $\langle \Delta Z_g \rangle$ and $\langle \Delta Z_r \rangle$ can be estimated from the empirical distributions shown in Figure 8, under the assumption of exponential distributions. Figure 10 shows that $\langle \Delta Z_g \rangle$ decreases slowly with Re, as expected from the typical scaling
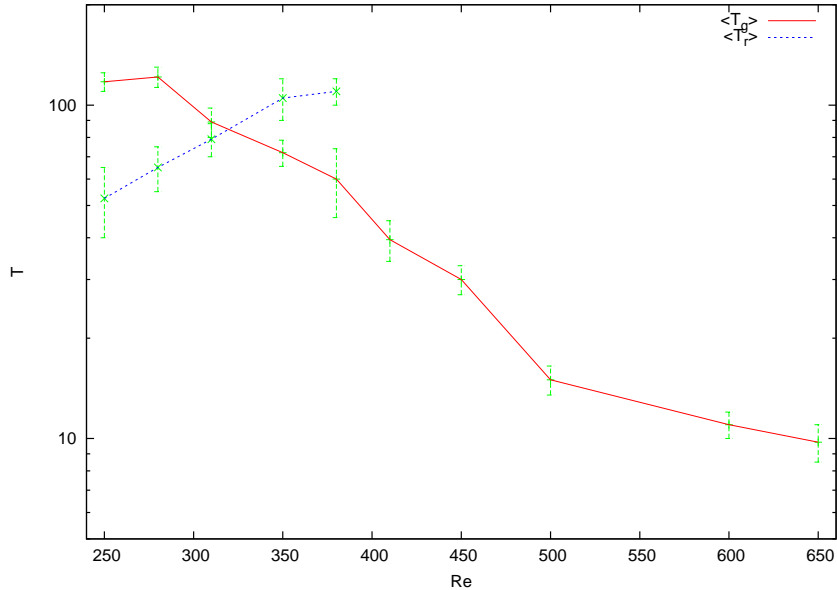
FIG. 9: Mean conditional waiting times $\langle T_g \rangle(Re)$ and $\langle T_r \rangle(Re)$.

of the streak width in viscous units general to all turbulent shear flows [34]. The quantity $\langle \Delta Z_r \rangle$, in the range where data are available, also decreases gently with Re. Rather than the expected high-Re trend, the most striking feature of Figure 10 is the tendency of both $\langle \Delta Z_g \rangle$ and $\langle \Delta Z_r \rangle$ to significantly increase at low Re, up to much larger values than the width of individual streaks. This confirms *a posteriori* the observation that multiple streaks can be either gained or lost brutally near the interface. This behaviour is consistent with an increase of the spanwise correlation length at low Re. The brutal increase also suggests to interpret large retreat events as a partial relaminarisation of the flow. In addition, the two values $\langle \Delta Z_g \rangle$ and $\langle \Delta Z_r \rangle$ are not equal, underlying the asymmetry between the g and r mechanisms.

3.3 First moments of the interface location

Let us denote $Z(t)$ the location of a single interface. Without loss of generality, it is assumed that the turbulent domain is on the left side of the interface. Consequently, r (resp. g) events correspond to negative jumps Δz (resp. positive jumps Δz). Recall that $P_{T_r}(\tau)$ and $P_{T_g}(\tau)$ are the probabilities that the interface at $Z(t)$ at time t will *not* undergo any motion of type r and g respectively, in the time interval $[t, t + \tau)$ with $\tau \geq 0$. We have
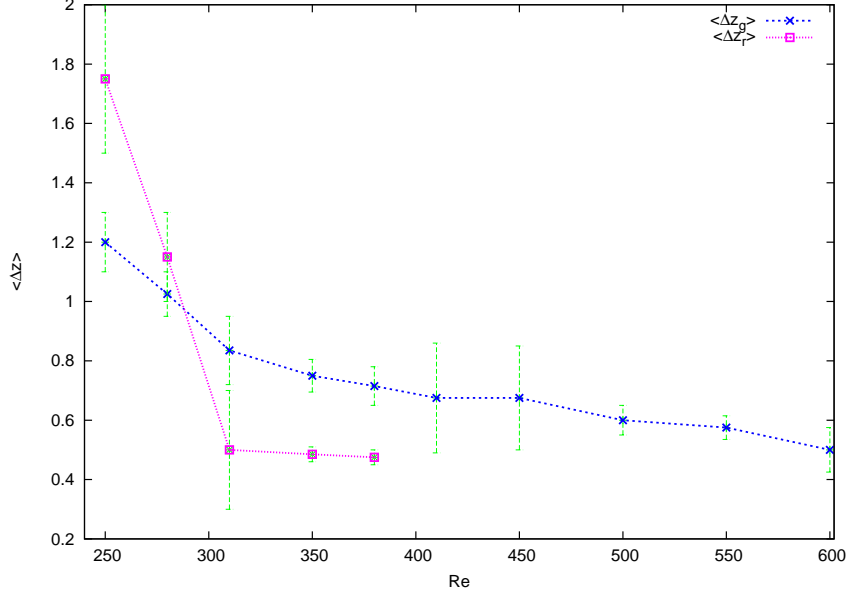
18

FIG. 10: Mean conditional jump lengths $\langle \Delta Z_g \rangle(Re)$ and $\langle \Delta Z_r \rangle(Re)$.

seen that the two distributions are reasonably approximated by exponential laws having respective average waiting times $\langle T_r \rangle$ and $\langle T_g \rangle$,

$$P_{T_r}(\tau) = \exp\left(-\tau/\langle T_r \rangle\right), \quad P_{T_g}(\tau) = \exp\left(-\tau/\langle T_g \rangle\right), \tag{2}$$

where $\langle T_r \rangle$ and $\langle T_g \rangle$ depend on Re. Therefore, the probability that the interface undergoes no motion in the time interval $[t, t+\tau)$ is the probability that r and g motion will not occur in this time interval, and is given by the product of the respective probabilities. Denoting this probability $P_T(\tau)$, we get

$$P_T(\tau) = P_{T_r}(\tau) \times P_{T_g}(\tau) = \exp\left(-\tau/\langle T \rangle\right), \quad \langle T \rangle = \frac{\langle T_r \rangle \langle T_g \rangle}{\langle T_r \rangle + \langle T_g \rangle}, \tag{3}$$

where $\langle T \rangle$ is the average waiting time between two consecutive motions (of any type r or g). Accounting for the orientation of interface, and introducing as $\pi_r(\Delta z)$ and $\pi_g(\Delta z)$ the probability density functions of the r and g jumps

$$\pi_r(\Delta z) = \begin{cases} 0, & \Delta z > 0 \\ \geq 0, & \text{otherwise} \end{cases}, \quad \pi_g(\Delta z) = \begin{cases} 0, & \Delta z < 0 \\ \geq 0, & \text{otherwise} \end{cases},$$

$$\int_{-\infty}^{+\infty} \pi_{r,g}(\Delta z) d\Delta z = 1. \tag{4}$$

we are now able to derive the probability $p(\tau, \Delta z) d\tau dz$ that the next move of the interface will occur between $[t+\tau, t+\tau+d\tau)$ with a (signed or oriented) displacement being in $[\Delta z, \Delta z+dz)$

19

(recall that $d\tau$ and dz are here infinitesimal). It is the product of the probability that no move happens in $[t, t+\tau)$, times the sum of the respective probabilities that a r or a g move occurs in $[t + \tau, t + \tau + d\tau)$ with value in $[\Delta z, \Delta z + dz)$. For a completely homogeneous Markovian process, the probability (to first order in $d\tau$) that a r move occurs in the time-interval $[t + \tau, t + \tau + d\tau)$ is given by $d\tau/\langle T_r \rangle$ (see [35, 36]), such that this motion with displacement in $[\Delta z, \Delta z + dz)$ has a probability $(\pi_r(\Delta z)/\langle T_r \rangle)\, d\tau dz$. By analogy for the g motion one obtains

$$p(\tau, \Delta z)d\tau dz = P_T(\tau) \times \Big(\frac{1}{\langle T_r \rangle}\pi_r(\Delta z) + \frac{1}{\langle T_g \rangle}\pi_g(\Delta z)\Big)d\tau dz. \tag{5}$$

Integrating over Δz the joint probability density function $p(\tau, \Delta z)$, we obtain the probability density function of the waiting time τ,

$$p_T(\tau) = \frac{1}{\langle T \rangle} \exp\big(-\tau/\langle T \rangle\big), \tag{6}$$

which corresponds to the τ-derivative of $(1 - P_T(\tau))$, as expected. Further, we will need the consolidated probability density function $p_\Delta(\Delta z)$ of the displacement. We observe that $p(\tau, \Delta z)$ can be written as the product of densities $p_T(\tau)$ and $p_\Delta(\Delta z)$, such that using (5) and (6) it comes

$$p_\Delta(\Delta z) = \frac{p(\tau, \Delta z)}{p_T(\tau)} = \frac{\langle T_g \rangle \pi_r(\Delta z) + \langle T_r \rangle \pi_g(\Delta z)}{\langle T_r \rangle + \langle T_g \rangle}. \tag{7}$$

We are now in position to derive exact expressions for the first moments of the interface location $Z(t)$. Assuming that the interface is at location z_0 at an initial time t_0, the average position at time $t > t_0$ is given by $\langle Z(t) \rangle = z_0 + \langle c \rangle (t - t_0)$, where the average velocity $\langle c \rangle$ is the ratio of the mean jump (first moment of p_Δ) with the mean waiting time $\langle T \rangle$. Using (7), we obtained the expression the average velocity

$$\langle c \rangle := \frac{1}{\langle T \rangle} \int_{-\infty}^{\infty} \Delta z\, p_\Delta(\Delta z)d\Delta z = \frac{1}{\langle T_r \rangle} \int_{-\infty}^{0} \Delta z\, \pi_r(\Delta z)d\Delta z + \frac{1}{\langle T_g \rangle} \int_{0}^{\infty} \Delta z\, \pi_g(\Delta z)d\Delta z$$
$$= \frac{\langle \Delta Z_r \rangle}{\langle T_r \rangle} + \frac{\langle \Delta Z_g \rangle}{\langle T_g \rangle} =: \langle c_r \rangle + \langle c_g \rangle, \tag{8}$$

where $\langle c_r \rangle = \langle \Delta Z_r \rangle / \langle T_r \rangle$ and $\langle c_g \rangle = \langle \Delta Z_g \rangle / \langle T_g \rangle$ are the signed (oriented) average velocities of the r and g events.

We observe that $\langle c \rangle$ is the direct sum of the averaged conditional velocities of the r and g motions, and not their sum weighted by the relative probabilities of the next motion being of type r or g.

Figure 11 shows the average front velocity $\langle c \rangle$ as a function of Re, along with the corresponding error bars. Also shown are the (unsigned) average velocities $\langle c_r \rangle$ and $\langle c_g \rangle$ of the r and g motions. The average front velocity $\langle c \rangle$ grows monotonically with Re for the present convention where r events correspond to negative jumps. $\langle c \rangle$ is equal to zero for a given value of $Re = Re_{c2} \approx 305 \pm 10$. The conclusion is clear: spanwise localised spots tend to shrink statistically for $Re \leq Re_{c2}$ while they expand for $Re \geq Re_{c2}$. The two threshold values Re_{c1} and Re_{c2} are expected to differ slightly given the effective asymmetry between g and r jump distributions. The discrepancy between these two quantities is nevertheless comparable to the accuracy of the measurements, thus we do not consider it necessary to discuss it in detail. Let us mention again the intriguingly good match with the experimentally and numerically obtained threshold value above which two-dimensional spots start to grow, found to be approximatively 325.

Note that $\langle c \rangle(Re)$ reaches a plateau corresponding to low but positive values of $\langle c \rangle$, indicating a slow average expansion of the turbulent spot, in the Re-interval $[320, 400]$. The existence of this plateau results directly from the competition between the two conditional velocities $\langle c_g \rangle$ and $\langle c_r \rangle$, which are also shown in Figure11 .

The trend for the large-Re behaviour of $\langle c \rangle(Re)$ is difficult to predict from the present data, in particular because of the rarity of r events that forced us to the simplification $\langle T_r \rangle = +\infty$ for $Re \geq 400$. However, we note that the values obtained experimentally for the spanwise front propagation [8, 9], restricted to comparable values of Re, are nearly one order of magnitude above the present data. As mentioned in Section 1, the quasi-1D geometry considered here differs from the case of fully localised turbulent spots by the absence of large-scale circulations around them [15, 16]. The mismatch in the front velocities could thus simply reflect the omission of advection by the secondary flow in the modelling. Another investigation focusing only on the purely spanwise propagation of a laminar-turbulent interface yields $\langle c \rangle \approx 0.08$ independently of Re [37]. The modelling used to derive this estimate is however based on the underlying assumption that Re is large. We have interpolated the values of $\langle c \rangle$ up to $Re \approx 600$ only, for which $\langle c \rangle \approx 0.05 \pm 0.01$. The estimate in Ref. [37] is thus consistent with the values in Fig. 11.
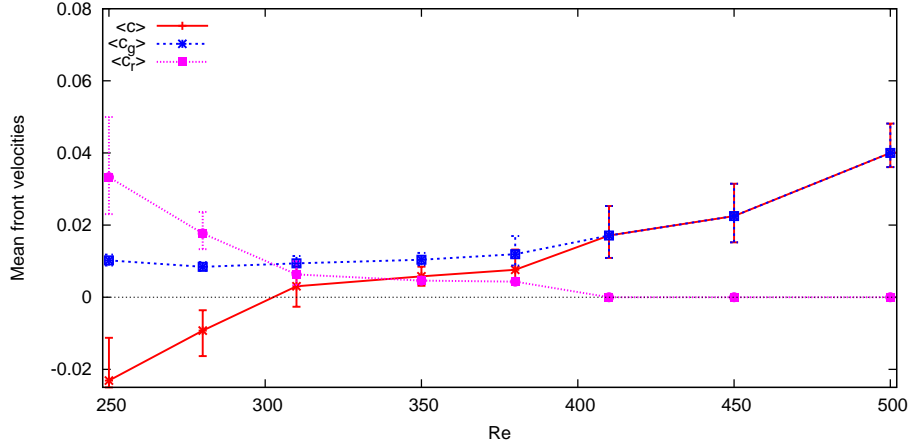
FIG. 11: Average front velocity $\langle c \rangle$ as a function of Re. Also provided are the (unsigned) average velocities of r and g events $\langle c_r \rangle (Re)$ and $\langle c_g \rangle (Re)$

.

In a similar way as for the average front location and velocity, one can derive exact expressions for the second order characterisation of $Z(t)$. Of particular importance is the variance of $Z(t)$, denoted $\sigma_Z^2(t) := \langle (Z(t) - \langle Z(t) \rangle)^2 \rangle$, which measures the spreading in the interface location about its mean. For completely homogeneous Markov processes, an explicit expression for $\sigma_Z^2(t)$ from the second moment of the displacement and characteristic time-scale is available [36]:

$$\sigma_Z^2(t) = \frac{(t - t_0)}{\langle T \rangle} \int_{-\infty}^{\infty} (\Delta z)^2 \, p_\Delta(\Delta z) d\Delta z, \qquad\qquad t_0 \le t. \qquad (9)$$

Accounting for the expression of the consolidated displacement probability density function in (7), the second moment of Δz expresses as

$$\int_{-\infty}^{\infty} (\Delta z)^2 \, p_\Delta(\Delta z) d\Delta z = \frac{\langle T_g \rangle}{\langle T_r \rangle + \langle T_g \rangle} \int_{-\infty}^{0} (\Delta z)^2 \, \pi_r(\Delta z) d\Delta z + \frac{\langle T_r \rangle}{\langle T_r \rangle + \langle T_g \rangle} \int_{0}^{\infty} (\Delta z)^2 \, \pi_r(\Delta z) d\Delta z$$
$$= \frac{\langle T_g \rangle \langle \Delta Z_r^2 \rangle}{\langle T_r \rangle + \langle T_g \rangle} + \frac{\langle T_r \rangle \langle \Delta Z_g^2 \rangle}{\langle T_r \rangle + \langle T_g \rangle},$$

$$(10)$$

where $\langle \Delta Z_{r,g}^2 \rangle$ are the second moments of the r and g displacements respectively. The expression for the variance of $Z(t)$ then becomes

$$\sigma_Z^2(t) = \left[\frac{\langle \Delta Z_r^2 \rangle}{\langle T_r \rangle} + \frac{\langle \Delta Z_g^2 \rangle}{\langle T_g \rangle} \right] (t - t_0), \qquad\qquad t_0 \le t. \qquad (11)$$

22

In addition, disregarding the extreme displacement values, we have seen that the distributions of r and g jumps can by approximated by exponential distributions; for such distributions we have $\langle \Delta Z_{r,g}^2 \rangle = 2\langle \Delta Z_{r,g} \rangle^2$, leading to the following approximation for the variance

$$\sigma_Z^2(t) = 2\langle D \rangle (t - t_0), \quad \langle D \rangle \approx \langle D_r \rangle + \langle D_g \rangle = \frac{\langle \Delta Z_r \rangle^2}{\langle T_r \rangle} + \frac{\langle \Delta Z_g \rangle^2}{\langle T_g \rangle}, \tag{12}$$

where $\langle D \rangle$ is the effective diffusion coefficient of the stochastic process.

Fig. 12 shows the effective diffusion coefficient $\langle D \rangle (Re)$ as approximated by (12). The quantity $\langle D \rangle$ is a measure of the statistical spreading rate of the front location. It can be seen that $\langle D \rangle$ exhibits a plateau for Re in the range $[320, 410]$. Interestingly, this plateau is located in the same range of Re values as the region of existence of the laminar-turbulent patterns reported in Refs. [12, 13]. Such patterns are certainly excluded from the present configuration precisely because of their obliqueness. However, it is natural to anticipate that the mechanisms responsible for the robustness and sustenance of the patterns locally imply statistical equilibrium for the associated fronts. This is verified here by the characteristics of the Re-plateau observed in the present computations: vanishing front velocity and minimal dispersion of the location of the interface.
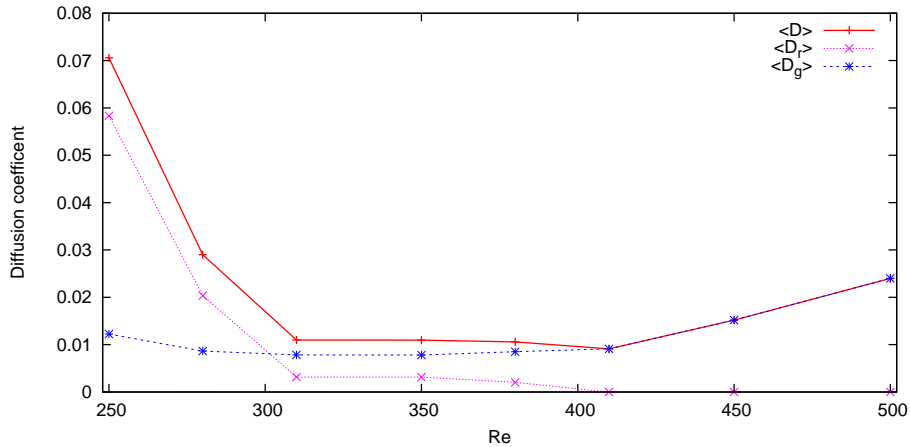

FIG. 12: Effective diffusion coefficient $\langle D \rangle$ of the interface motion as a function of Re. Also provided are the diffusion coefficients $\langle D_r \rangle (Re)$ and $\langle D_g \rangle (Re)$ of the r and g events.

3.4 Data-driven stochastic model

This subsection suggests a simple stochastic model based on the data from the previous DNS. In the spirit of Ref. [38], this model allows for very low-cost simulation of the dynamics of multiple interfaces, with the ability of tackling arbitrary large domains over times unreachable by DNS, while keeping the stochastic properties of the phenomenon. Let us consider an absorbing medium (*i.e.* laminar for $|z| \to \infty$) with $2n$ distinct interfaces, such that there are n turbulent spots; we assume that the interfaces are ordered as $Z_1(t) < \cdots < Z_{2n}(t)$, so that $Z_{2i-1}(t)$, $i = 1, \ldots, n$, separate a laminar domain on its left-side from a turbulent domain on its right-side (and conversely for interfaces with even indices $Z_{2i}(t)$). The stochastic evolution of this system of interfaces is simulated as follows. Starting from the configuration of the interfaces at an initial time $t = t_0$, we first draw from the exponential waiting time distribution of the system, with mean $\langle T \rangle/(2n)$, the elapse time τ to the next event. We then select at random, with equal probability, one of the $2n$ interfaces, say Z_i.

We further select at random the type of event (r or g), with respective probabilities Π_g and Π_r given by (using the notation above)

$$\Pi_r = \int_{-\infty}^{0} p_\Delta(\Delta z) d\Delta z = \frac{\langle T_g \rangle}{\langle T_r \rangle + \langle T_g \rangle}, \quad \Pi_g = \int_{0}^{+\infty} p_\Delta(\Delta z) d\Delta z = \frac{\langle T_r \rangle}{\langle T_r \rangle + \langle T_g \rangle}. \quad (13)$$

Assuming that we selected a g event (the case for r is similar), we update the system according to

$$t \longleftarrow t + \tau, \quad Z_i \longleftarrow Z_i + (-1)^i \eta, \quad (14)$$

where η is drawn at random from the exponential fit of the (unsigned) distribution $P_{\Delta g}$. The advancement of the system state is completed after checking that none of the interfaces crossed with its two neighbors. Specifically, using $Z_0 = -\infty$ and $Z_{2n+1} = +\infty$, if after the displacement of the i-th interface we have $Z_i \leq Z_{i-1}$ (resp. $Z_i \geq Z_{i+1}$) the interfaces Z_{i-1} and Z_i (resp. Z_i and Z_{i+1}) are removed from the set of interfaces and we affect new indices to the remaining ones ($n \leftarrow n - 2$). We repeat this sequence until t reaches a prescribed final time or, eventually, until all interfaces have disappeared.

In Figure 13, we present examples of numerical simulations corresponding to $Re = 250$, 350 and 450. The simulations use the exponential distributions fitted on the data from the DNS at the corresponding Reynolds numbers. The first column shows for the three

values of Re the evolution in time of a single turbulent spot, together with the classical statistical representation of the 99% confidence intervals in the interface locations (using bounds $\langle Z_i(t) \rangle \pm 3\sigma_{Z_i}(t)$). The second column shows the evolutions of an initial set of 20 turbulent spots, where two consecutive interfaces are initially set at a distance irregularly distributed in the range $[50, 150]$. For $Re = 250$ (top row), we observe that all turbulent spots have disappeared after a time $\simeq 4,000$. For $Re = 350 > Re_{c2}$, none of the turbulent spots has disappeared, contrary to most of the inner laminar domains which have vanished at the end of the simulation time $t - t_0 = 10^4$, although their average survival time is quite long. At $Re = 450$ (bottom row), all inner laminar domains have disappeared after a time $\simeq 3,000$, giving a unique turbulent spot that continuously extends with time (recall that for $Re > 400$ no retreat event is modeled since we set $\langle T_r \rangle = +\infty$). Globally, the stochastic simulator reproduces satisfactorily the dynamics observed in the DNS, except for the large-scale relaminarisation events at the lowest Re, because of the fitted exponential laws that disregard the large jumps associated to rare relaminarisation events. In addition, the simulator lacks the probability of local relaminarisation *inside* turbulent spots. We plan to improve the stochastic simulator in the future to incorporate the missing features and sample the empirical distributions instead of the fitted ones. This will however require further Navier–Stokes simulations to extract additional statistical information.
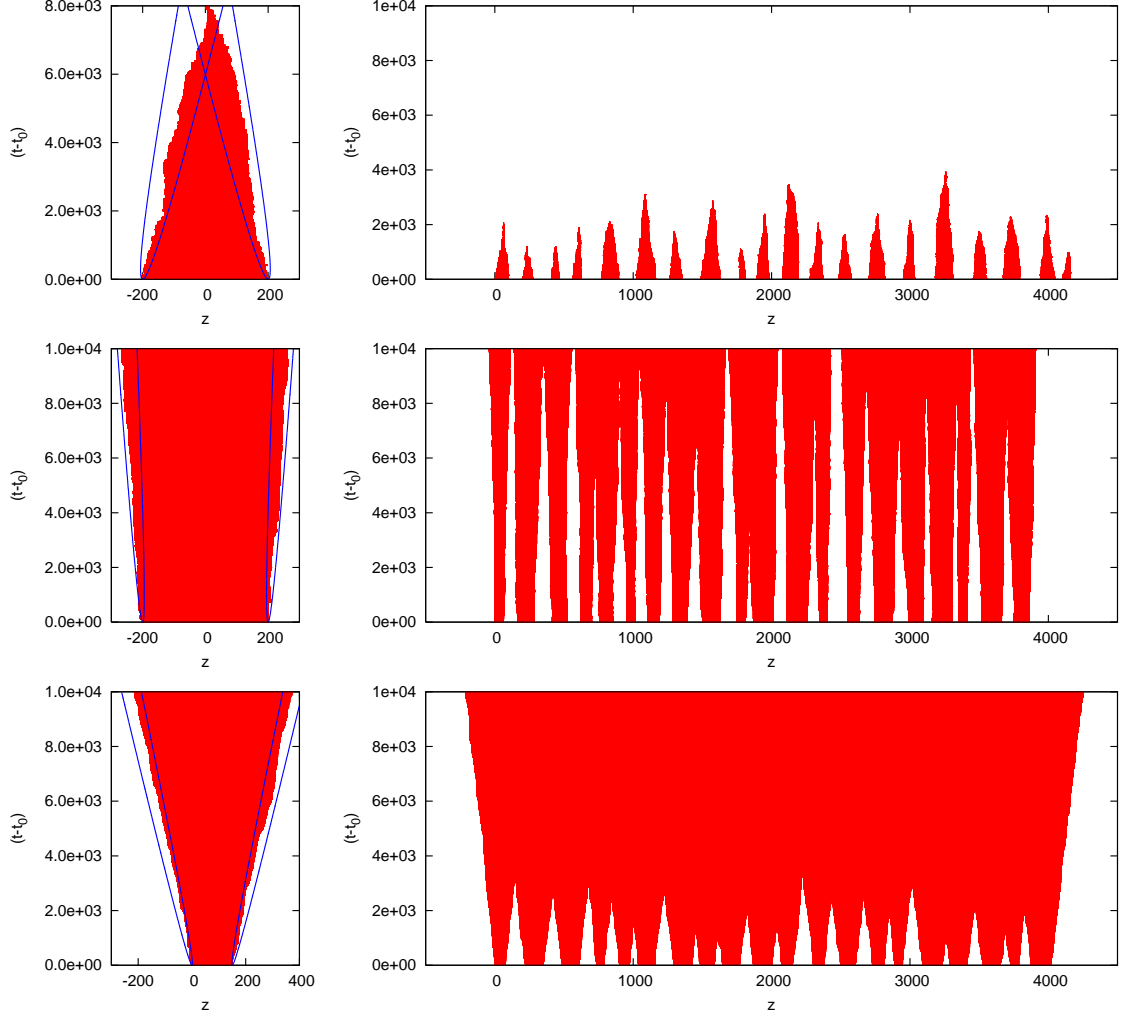
FIG. 13: Example of stochastic simulations at $Re = 250$ (first row), 350 (second row) and 450 (third row). Left column: time evolution of a single turbulent spot (red (dark) domain) together with statistical bounds $\langle Z_i(t) \rangle \pm 3\sigma_{Z_i}(t)$ for the left and right interface location (plain lines). Right column: time evolution of a set of 20 turbulent spots (red (dark) domains).

4. DETERMINISTIC FRONT MOTION AT LOW REYNOLDS NUMBERS

The results of the previous section point out that the assumption for Gaussianity breaks down for the lowest values of Re. From $Re \sim 280$ down to $Re = 217 \pm 1$, some unexpected non-trivial (not necessary "turbulent") dynamics is observed, characterised by phases of regular growth over times much longer than predicted by the low-Re extrapolation of the previous distributions. The fact that a non-trivial flow could be sustained in that geometry at such low values of Re was already pointed out in Ref. [20]. At the lowest values of Re near 217, the dynamics reduces to the competition between these growth phases and brutal retreat events, as is suggested by the space-time diagrams for $Re = 220$ and $Re = 225$ in Fig. 14.
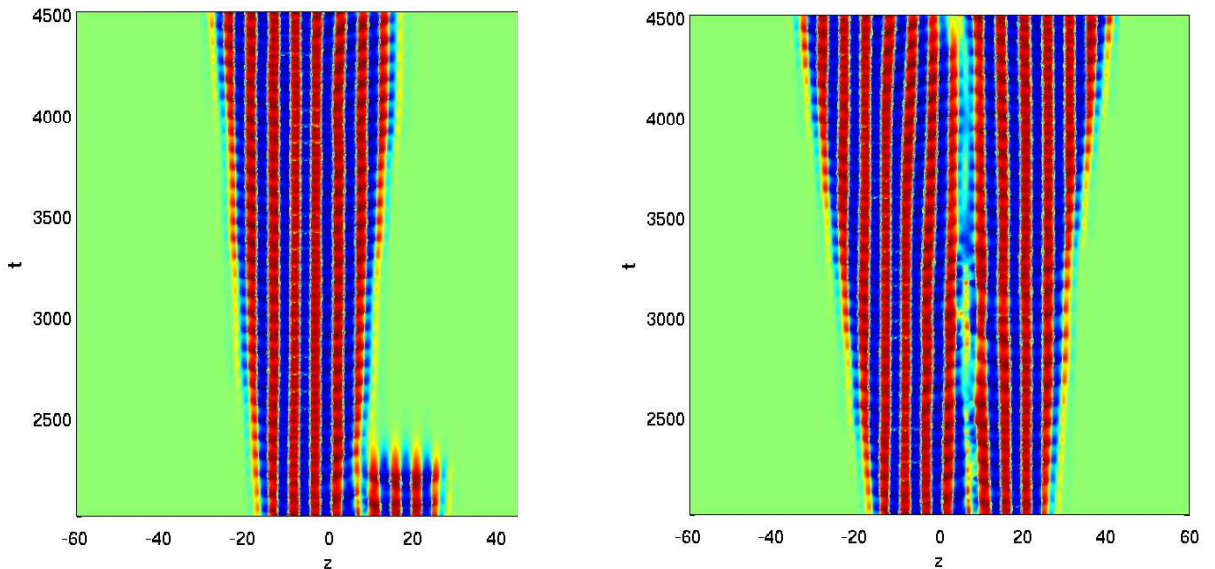

FIG. 14: Space-time (z,t) diagrams for the quantity $Y(z,t)$; Re=220 (left) and Re=225 (right)

These long growth phases are very reminiscent of the depinning transition predicted in the vicinity of a snaking region in extended one-dimensional systems (for a recent review, see also Ref. [39]). If the system is parametrised by a governing parameter r (here the Reynolds number Re), there is a so-called snaking region $[r_1, r_2]$ with a multiplicity of exact localised states pinned to a periodic array of regular cells (here the streaks). Depinning outside the snaking region causes temporal expansion or collapse of the initially localised pattern. Expansion (resp. collapse) occurs in two ways: either through nucleation (resp. annihilation) of new cells near the interface at a steady rate, in the case of regular homoclinic

27

snaking (see Fig.14 in Ref. [40]), or through phase slips in a central region far from the interfaces, as in the case of defect-mediated snaking (see Fig.21 in Ref. [41]). A closer zoom of Fig. 14 reveals that the new streaks are nucleated precisely near the interface, and at a seemingly steady rate, thus favouring the hypothesis for regular homoclinic snaking. Homoclinic snaking is observed in situations where a non-trivial ("patterned") steady state with a spatially periodic structure bifurcates subcritically from a trivial homogeneous ("laminar") solution. Plane Couette flow definitely falls into this category, the pattern state being associated with the non-trivial unstable solutions found so far in small periodic domains [42, 43]. The non-trivial branch then bifurcates into two branches which can be traced down the governing parameter and begin to intertwingle inside the range $[r_1, r_2]$, giving rise to a multiplicity of steady/travelling localised states pinned to the non-localised patterned state. Analysis in the case of the Swift-Hohenberg equations has shown that for $0 < \delta = r - r_2 \ll 1$, depinning of the fronts occurs, i.e. the fronts are no longer stationary yet drift so that the patterned state invades the whole domain with a velocity scaling as $O(\delta^{\frac{1}{2}})$ (see Fig.14 in Ref. [40]).

Recently, Schneider et al. [44] have considered the case of PCF with periodic boundary conditions in x and z with extension in the z direction, taking $(L_x, L_z) = (4\pi, 16\pi)$. This is qualitatively very similar to the quasi-1D geometry considered here. They have identified a homoclinic snaking region in the interval $Re \in [Re_{s1} : Re_{s2}] \approx [170 : 175]$, however the values of Re reported in that study depend strongly on the value of L_z. For the case at hand ($L_z = 10.417 \approx 3.3\pi$), the snaking interval is $[207.4 : 213.2]$ [45].

In order to verify that the long growth phases are related to the depinning transition, a set of simulations has been analysed for several values of Re between 190 and 280, all starting from the same turbulent state obtained in a previous run at $Re = 250$. Since we are interested here in long growth phases rather than on the retreat or growth events on a short time-scale, we have deliberately selected only growth events with a constant velocity on a time scale $T > 1000$. An interpolation is then performed directly from space-time- diagrams such as those in fig. 14, yielding the front velocity $c = \Delta z / T$ as a function of Re. From Fig. 15 it can be inferred that c obeys a scaling $c(Re) = O((Re - Re_{s2})^{\frac{1}{2}})$, as suggested in Ref. [40]. Interpolation from Fig. 15 yields the value $Re_{s2} = 216 \pm 1$ for the rightmost extremity

of the snaking region. This is in very good agreement with the data from Ref. [45] (despite the fact that the two compared systems use distinct values for L_z). There is little ambiguity that the very regular regime of sustained growth observed for $Re < 280$ corresponds to a depinning transition, justifying de facto its deterministic nature.
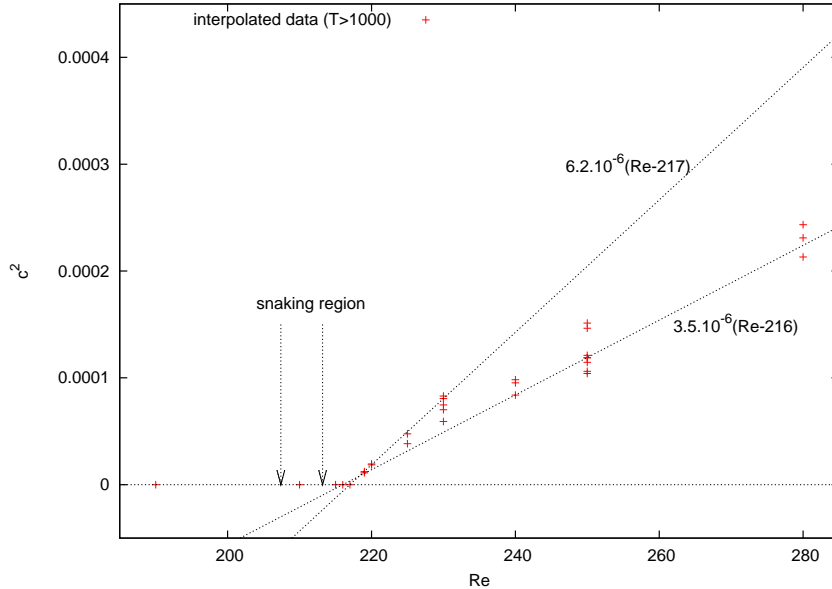

FIG. 15: Mean velocity squared c^2 associated to deterministic events over large times $T > 1000$ (see text). The expected $c^2 \sim O(Re)$ scaling is indicated for comparison, along with the exact location of the snaking region.

CONCLUSIONS

We have investigated the dynamics of a laminar-turbulent interface in plane Couette flow, in the special case where the interface is parallel to the mean flow direction. The motion appears to be stochastic in nature, and follows a Gaussian law above $Re \geq 280$, with an average speed (into the laminar region) increasing from negative values at low Re to positive values at higher Re. We observe the presence of a plateau for $Re \approx [320 : 410]$, where the front velocity is close to zero and the associated diffusion coefficient is minimal. Interestingly, this plateau corresponds to the range of Re at which robust laminar-turbulent patterns are observed in experiments and large-scale simulations. The relevance of this observation to the description of the spreading of fully localised turbulent spots should however be analysed
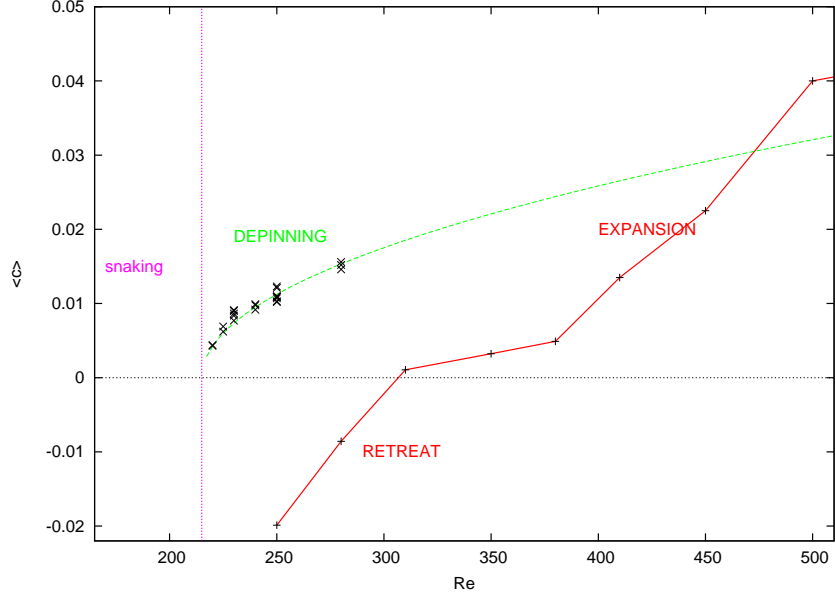
29

FIG. 16: Mean velocity $\langle c \rangle$ of a front vs. Re. The green (dashed) line corresponds to deterministic expansion (actual data represented by black crosses), the red (plain) curve to stochastic motion (actual data represented by right crosses).

with caution, precisely because the configuration at hand deliberately ignores some typically three-dimensional effects, the most obvious candidate being the effect of a large-scale flow induced by the spatial localisation of the Reynolds stresses [15, 16]. Even if the front velocity calculated here is not strictly zero within the plateau, there is a possibility that the extra advection by the large-scale flow would exactly balance the motion of the fronts and thus explain the steadiness of the patterns.

By pushing our statistical analysis to lower values of Re, we have encountered an unexpected regime where the front motion appears sometimes locked to a seemingly deterministic dynamics. This growth regime ($c > 0$) contrasts strongly with the expected negative value for the front velocity suggested by the interpolation of $\langle c \rangle (Re)$ in Fig. 11. From the results shown in Fig. 15, we interpret this deterministic regime as a depinning transition from the homoclinic snaking regime already identified using an other approach [44]. Thus for the lowest values of Re in our investigation, stochasticity is observed to compete with a deterministic dynamics (see Figure 16). Whether stochastic and deterministic "branches" bifurcate one from another or whether these are two disconnected phenomena remains to be investigated. No extension of the homoclinic snaking scenario to the fully localised plane

Couette spots has been suggested so far. Provided such an extension it would be interesting to test the relevance of this deterministic dynamics to fully localised spots.

Acknowledgements

―――――――

[1] POMEAU, Y., 1986 Front motion, metastability and subcritical bifurcations in hydrodynamics. *Physica D*, **23**, 3-11

[2] EMMONS, H. W., 1951 The laminar-turbulent transition in a boundary layer. Part I. *J. Aerosol. Sci.*, **18**, 490

[3] COLES, D., 1965 Transition in circular Couette flow. *J. Fluid Mech.*, **21**, 385-425

[4] VAN ATTA, C.W., 1966 Exploratory measurements in spiral turbulence, *J. Fluid Mech.*, **25**, 495-512

[5] WYGNANSKI, I. J., CHAMPAGNE, F. H., 1973 On transition in a pipe. Part 1. The origin of puffs and slugs and the flow in a turbulent slug, *J. Fluid Mech.*, **59**, 281-351.

[6] ROMANOV, V.A., 1973 Stability of plane-parallel Couette flow. *Funct. Anal. Appl.*, **7**, 137-146

[7] DAVIAUD, F., HEGSETH J.J. & BERGÉ P., 1992 Subcritical transition to turbulence in plane Couette flow. *Phys. Rev. Lett.*, **69**, 2511-2514

[8] TILLMARK, N. & ALFREDSSON, P.H., 1992 Experiments on transition in plane Couette flow, *J. Fluid Mech.*, **235**, 89-102

[9] DAUCHOT, O. & DAVIAUD, F., 1995 Finite amplitude perturbation and spots growth mechanism in plane Couette flow. *Phys. Fluids*, **7**, 335-343

[10] HEGSETH, J.J., 1996 Turbulent spots in plane Couette flow. *Phys. Rev. E*, **5**, 4915

[11] MANNEVILLE, P., 2005 Modeling the Direct Transition to Turbulence.. *Laminar-Turbulent Transition and Finite Amplitude Solutions, ed. T. Mullin, R.R. Kerswell, Springer Netherlands*

[12] DUGUET, Y., SCHLATTER, P. & HENNINGSON, D.S., 2010 Formation of turbulent patterns near the onset of transition in plane Couette flow. *J. Fluid Mech.*, **650**, 119-129

[13] PRIGENT, A., 2001 La spirale turbulente: motif de grande longueur d'onde dans les écoulements cisaillés turbulents. *PhD Thesis, Université Paris XI*

[14] PRIGENT, A., GRÉGOIRE, G., CHATÉ, H., DAUCHOT, O. & VAN SAARLOS, W., 2002 Large-scale finite-wavelength modulation within turbulent shear flows. *Phys. Rev. Letters*, **89**, 014501

[15] LUNDBLADH, A. & JOHANSSON, A.V., 1991 Direct simulation of turbulent spots in plane Couette flow. *J. Fluid Mech.*, **229**, 499-516

[16] LAGHA, M. & MANNEVILLE, P., 2007 Modeling of plane Couette flow. I. Large scale flow around turbulent spots. *Phys. Fluids*, 19, 094105

[17] SCHUMACHER, J. & ECKHARDT, B., 2001 Evolution of turbulent spots in plane shear flow. *Phys. Rev. E*, **63**, 046307.

[18] GAD-EL-HAK, M., BLACKWELDER, R. F., & RILEY, J. R., 1981 On the growth of turbulent regions in laminar boundary layers. *J. Fluid Mech.*, **110** 73-95

[19] CHEVALIER, M., SCHLATTER, P., LUNDBLADH, A. & HENNINGSON, D. S., 2007 A Pseudo-Spectral Solver for Incompressible Boundary Layer Flows. *Technical report TRITA-MEK 2007:07, KTH Mechanics, Stockholm, Sweden*

[20] BARKLEY, D. & TUCKERMAN, L.S., 2005 Turbulent-laminar patterns in plane Couette flow. *Laminar-Turbulent Transition and Finite Amplitude Solutions, ed. T. Mullin, R.R. Kerswell, Springer Netherlands*

[21] SCHNEIDER, T.M., MARINC, D. & ECKHARDT, B., 2010 Localized edge states nucleate turbulence in extended plane Couette cells. *J. Fluid Mech.*, **646**, 441-451

[22] SCHNEIDER, T. M., GIBSON, J. F. & BURKE, J., 2010 Snakes and Ladders: Localized Solutions of Plane Couette Flow. *Phys. Rev. Lett.*, **104**, 104501

[23] DUGUET, Y., SCHLATTER, P. & HENNINGSON, D.S., 2009 Localized edge states in plane Couette flow. *Phys. Fluids*, **21**, 111701

[24] JIMENEZ, J., KAWAHARA, G., SIMENS, M. P., NAGATA, M. & SHIBA, M., 2005 Characterization of near-wall turbulence in terms of equilibrium and bursting solutions. *Phys. Fluids*, **17**, 015105

[25] KAWAHARA, G., KIDA, S., 2001 Periodic motion embedded in plane Couette turbulence:

regeneration cycle and burst. *J. Fluid Mech.*, **449**, 291–300

[26] TOH, S. & ITANO, T., 2003 A periodic-like solution in channel flow, *J. Fluid Mech.*, **481**, 67-76

[27] BOTTIN, S., DAUCHOT, O., DAVIAUD, F. & MANNEVILLE, P, 1998 Experimental evidence of streamwise vortices as finite amplitude solutions in transitional plane Couette flow. *Phys. Fluids*, **10**, 2597-2607

[28] VAN SAARLOOS, W., 2003 Front propagation into unstable states. *Phys. Rep.*, **386**, 29-222.

[29] MONTROLL, E. W. & WEISS, G. H., 1965 Random walks on lattices. *J. Math. Phys.*, **6**, 167

[30] CHATÉ & MANNEVILLE, P., 1987 Intermittence spatio-temporelle et automates cellulaires probabilistes. *C.R. Acad. Sci. Paris*, **304**, 609

[31] FA, K. S. & MENDES, R. S., 2010 A continuous time random walk model with multiple characteristic times. *J. Stat. Mech.*, P04001

[32] AVILA, K., MOXEY, D., DE LOZAR, A., AVILA, M., BARKLEY, D. & HOF, B., 2011 The onset of turbulence in pipe flow. *Science*, **8**, 192-196

[33] BARKLEY, D., 2011 Simplifying the complexity of pipe flow. *submitted to Phys. Rev. E*

[34] KLINE, S. J., REYNOLDS, W. C., SCHRAUB, F. A. & RUNSTADLER, P. W., 1967 The structure of turbulent boundary layers. *J. Fluid Mech.*, **30**, 741.

[35] GARDINER, C.W., 1997 Handbook of stochastic methods. 2nd Edition, *Springer Series in Synergetics, Springer, Berlin*

[36] GILLESPIE, D.T., 1992 Markov processes, an introduction for physical scientists. *Academic Press Inc., San Diego*

[37] TAKAKI, R., 1987 Spanwise propagation of turbulence in the plane Couette flow, *Fluid Dynamics Research*, **1**, 229-236

[38] VINOD, N. & GOVINDARAJAN, R., 2004 Pattern of breakdown of laminar flow into turbulent spots, *Phys. Rev. Lett.*, **93**, 144501

[39] DAWES, J. H. P., 2010 The emergence of a coherent structure for coherent structures: localized states in nonlinear systems. *Phil. Trans. R. Soc. A*, **368**, 3519-3534

[40] BURKE, J. & KNOBLOCH, E., 2006 Localized states in the generalized Swift-Hohenberg equation. *Phys. Rev. E* , **73**, 056211

[41] MA, Y., BURKE, J. & KNOBLOCH, E., 2010 Defect mediated snaking in the forced complex Ginzburg-Landau equation. *Physica D*, 239, 1867.

[42] GIBSON, J. F., HALCROW, J. & CVITANOVIĆ, P., 2009 Equilibrium and traveling-wave solutions of plane Couette flow *J. Fluid Mech.*, **638**, 1-24

[43] WALEFFE, F., 1998 Three-dimensional coherent states in plane shear flows, *Phys. Rev. Letters*, **81**, 19, 4140–4143.

[44] SCHNEIDER, T. M., GIBSON, J. F. & BURKE, J., 2010 Snakes and Ladders: Localized Solutions of Plane Couette Flow. *Phys. Rev. Lett.*, **104**, 104501

[45] J.F. GIBSON, 2011 private communication.